Nickel-deficient Stannides $Eu_2Ni_{2-x}Sn_5$ – Structure, Magnetic Properties, and Mössbauer Spectroscopic Characterization

Thomas Harmening, Matthias Eul, and Rainer Pöttgen

Institut für Anorganische und Analytische Chemie and NRW Graduate School of Chemistry, Westfälische Wilhelms-Universität Münster, Corrensstraße 30, 48149 Münster, Germany

Reprint requests to R. Pöttgen. E-mail: pottgen@uni-muenster.de

New nickel-deficient stannides $Eu_2Ni_{2-x}Sn_5$ were synthesized by induction melting of the elements in sealed tantalum tubes. The solid solution was studied by X-ray powder diffraction and two crystal structures were refined on the basis of X-ray diffractometer data: *Cmcm*, $a = 466.03(4)$, $b = 3843.1(8)$, $c = 462.92(9)$ pm, $wR2 = 0.0469$, 692 F^2 values, 39 variables for $Eu_2Ni_{1.49(1)}Sn_5$ and $a = 466.11(9)$, $b = 3820.1(8)$, $c = 462.51(9)$ pm, $wR2 = 0.0358$, 695 F^2 values, 39 variables for $Eu_2Ni_{1.35(1)}Sn_5$. This new structure type can be considered as an intergrowth structure of $CaBe_2Ge_2$- and CrB-related slabs. The striking structural motifs are nickel-centered square pyramids which are condensed *via* common corners and edges. The layers of condensed $NiSn_5$ units are separated by the europium atoms. The Ni1 sites within the $CaBe_2Ge_2$ slabs show significant defects which leads to split positions for one tin site. $Eu_2Ni_{1.50}Sn_5$ shows Curie-Weiss behavior and an experimental magnetic moment of 7.74(1) μ_B / Eu atom, indicating stable divalent europium, as is also evident from ^{151}Eu Mössbauer spectra. Antiferromagnetic ordering is detected at 3.5 K.

Key words: Europium, Stannide, Magnetic Properties, Mössbauer Spectroscopy

Introduction

Due to the almost similar ionic radii [1] of Sr^{2+} (112 pm) and Eu^{2+} (109 pm), several strontium and divalent europium compounds are isotypic. Prominent examples in the field of ionic compounds are the pairs SrO and EuO [2] with rocksalt structure, as well as Eu_3O_4 [3] and its strontium-substituted variant $SrEu_2O_4$ [3]. Such pairs also exist in the field of strontium and europium intermetallics. Recently reported compounds are $SrRhIn_2$ [4] and $EuRhIn_2$ [5], or the stannides SrPdSn / EuPdSn and SrPtSn / EuPtSn [6 – 10] with TiNiSi-type structure. However, in these stannides, the slight differences in size between strontium and europium already lead to different distortions within the three-dimensional transition metal (T)–tin networks. This is even more pronounced in the structures of SrAuSn [10] and EuAuSn [11]. Both stannides crystallize with a KHg_2-type subcell, but again, the small differences in the Sr^{2+} and Eu^{2+} radii force formation of a different superstructure, resulting in differently ordered and stacked Au_3Sn_3 hexagons.

In some cases, formation of isotypic compounds with strontium and europium does not occur. Tiny differences in chemical bonding then favor different

structural motifs. Such behavior has been observed in the tin-rich parts of the Sr-Au-Sn and Eu-Au-Sn systems. $SrAuSn_2$ [12] crystallizes with an incommensurately modulated structure that derives from the $CeNiSi_2$ type, while with europium a more tin-rich stannide $Eu_2Au_2Sn_5$ [13] is formed.

In the course of our systematic studies on structure-property relationships of intermetallic europium compounds [14 – 16, and refs. therein] we are searching for isotypic europium compounds for known strontium-transition metal stannides. Keeping the possibility for Sr/Eu substitution in mind we tried to synthesize a europium-based analog to $SrNiSn_3$ and $BaNiSn_3$ [17]. These attempts, however, resulted in the formation of the new stannide $Eu_2Ni_{2-x}Sn_5$ ($x \approx 0.5 - 0.7$). The structure and properties are reported herein.

Experimental Section

Synthesis

Starting materials for the synthesis of the $Eu_2Ni_{2-x}Sn_5$ samples were sublimed ingots of europium (Johnson Matthey), nickel wire ($\varnothing$ 0.38 mm, Johnson Matthey), and tin granules (Merck), all with stated purities better than 99.9 %. The europium ingots were cut into smaller pieces in a glove

box and kept in Schlenk tubes under argon prior to the reactions. The argon was purified before over molecular sieves, silica gel, and titanium sponge (900 K). The elements were weighed in the 2 : 1.5 : 5 atomic ratio and sealed in tantalum ampoules under an argon pressure of 700 mbar in an arc-melting apparatus [18]. The tantalum ampoules were subsequently placed in the water-cooled sample chamber of an induction furnace [19], heated to 1300 K and kept at that temperature for 30 min. Finally, the temperature was rapidly lowered to 900 K, and the samples were annealed at that temperature for another 3 h, and then cooled within the furnace after the power was switched off. No reaction with the container material was observed. The compact light-gray pieces and the dark-gray powder were stable in air. For crystal growth a sealed tantalum ampoule containing the elements in a 2 : 1.5 : 5 atomic ratio was sealed in an evacuated quartz tube. This was heated in a tube furnace to 1170 K and slowly cooled within 8 d to ambient temperature.

EDX data

The single crystals investigated on the diffractometer and the bulk samples were analyzed using a LEICA 420 I scanning electron microscope with EuF_3, Ni and Sn as standards. No impurity elements heavier than sodium (detection limit of the instrument) were observed. The compositions determined semiquantitatively by EDX were in good agreement with the compositions refined from the single crystal X-ray data.

X-Ray powder and single-crystal diffraction

The polycrystalline samples were characterized by Guinier patterns (imaging plate detector, Fujifilm BAS-1800) with $CuK\alpha_1$ radiation and α-quartz (a = 491.30, c = 540.46 pm) as an internal standard. Correct indexing of the diffaction lines was ensured through intensity calculations [20]. The orthorhombic lattice parameters of the sample prepared in the induction furnace were refined by least-squares calculations yielding a = 465.2(7), b = 3820(3), and c = 464.8(4) pm, in good agreement with the single crystal lattice parameters of $Eu_2Ni_{1.35(1)}Sn_5$.

High-quality crystals were selected from both crushed samples. They were first investigated *via* Laue photographs on a Buerger camera (white Mo radiation) in order to check their quality. Intensity data were collected with graphite-monochromatized $MoK\alpha$ radiation on an IPDS-II diffractometer in oscillation mode. Numerical absorption corrections were applied to the data sets. All relevant crystallographic data for the data collections and evaluations are listed in Table 1.

Structure solution and refinement

Careful examination of the data sets readily revealed C-centered orthorhombic lattices, and the additional systematic extinctions $h0l$ only observed for $h, l = 2n$ led to space

groups *Cmcm* and *Cmc2₁*, of which the centrosymmetric group was found to be correct in the structure refinements. The starting atomic parameters were deduced from an interpretation of Direct Methods with SHELXS-97 [21], and both structures were refined using SHELXL-97 [22] (full-matrix least-squares on F^2) with anisotropic atomic displacement parameters for all atoms. These refinements readily revealed two major anomalies, *i.e.* (i) the Ni1 sites showed too large equivalent isotropic displacements parameters, indicating defects, and (ii) the Sn5 sites showed extreme displacement parameters U_{22} (*e.g.* 1777(49) pm² for the $Eu_2Ni_{1.35(1)}Sn_5$ crystal). In the following least-squares cycles we refined the structures with free Ni1 occupancy parameters and introduced Sn5A and Sn5B split positions which were refined with isotropic (and constrained) displacements parameters. As a check for the correct composition, the other occupancy parameters were refined in separate series of least-squares cycles. These sites were fully occupied within two standard deviations, and in the final cycles the ideal occupancy parameters were assumed again for these sites.

The refined compositions were $Eu_2Ni_{1.35}Sn_5$ and $Eu_2Ni_{1.49}Sn_5$ for the crystals from the induction-melted sample and the one prepared in the tube furnace, respectively. The final difference Fourier syntheses were flat (Table 1). The positional parameters and interatomic distances are listed in Tables 2 and 3.

Further details of the crystal structure investigations may be obtained from Fachinformationszentrum Karlsruhe, 76344 Eggenstein-Leopoldshafen, Germany (fax: +49-7247-808-666; e-mail: crysdata@fiz-karlsruhe.de, http://www.fiz-informationsdienste.de/en/DB/icsd/depot_anforderung.html) on quoting the deposition numbers CSD-420972 ($Eu_2Ni_{1.49}Sn_5$) and 420971 ($Eu_2Ni_{1.35}Sn_5$).

Magnetic measurements

15.513 mg of the $Eu_2Ni_{1.5}Sn_5$ sample were packed in kapton foil and attached to the sample holder rod of a VSM for measuring the magnetic properties in a Quantum Design Physical-Property-Measurement-System in the temperature range 2.1 – 305 K with magnetic flux densities up to 80 kOe.

¹¹⁹Sn and ¹⁵¹Eu Mössbauer spectroscopy

The 21.53 keV transition of ¹⁵¹Eu with an activity of 130 MBq (2 % of the total activity of a ¹⁵¹Sm:EuF_3 source) was used for the ¹⁵¹Eu Mössbauer spectroscopy studies. A $Ca^{119m}SnO_3$ source was available for the ¹¹⁹Sn investigations, and a palladium foil of 0.05 mm thickness was used to reduce the tin K X-rays concurrently emitted by this source. The measurements were performed in the usual transmission geometry in commercial helium bath and flow cryostats. The temperature of the absorber could be varied from 4.2 to 300 K. The sources were kept at r. t. in all experiments. The

Atom	Occ.	x	y	z	U_{11}	U_{22}	U_{33}	U_{eq}
$Eu_2Ni_{1.49(1)}Sn_5$								
Eu1		0	0.81769(1)	1/4	128(3)	116(2)	126(2)	123(1)
Eu2		0	0.54802(1)	1/4	129(3)	124(3)	134(2)	129(1)
Ni1	0.482(7)	0	0.72828(7)	1/4	176(17)	157(16)	185(15)	173(10)
Ni2		0	0.91216(3)	1/4	116(6)	107(5)	109(5)	111(3)
Sn1		0	0.97762(2)	1/4	223(4)	101(3)	89(3)	138(2)
Sn2		0	0.25017(3)	1/4	182(4)	389(5)	204(4)	258(2)
Sn3		0	0.38403(2)	1/4	88(3)	170(3)	155(3)	137(2)
Sn4		0	0.11588(2)	1/4	143(4)	190(4)	71(3)	135(2)
Sn5A	0.528(2)	0	0.66497(5)	1/4	–	–	–	143(2)
Sn5B	0.472(2)	0	0.68132(5)	1/4	–	–	–	143(2)
$Eu_2Ni_{1.35(1)}Sn_5$								
Eu1		0	0.81780(3)	1/4	106(3)	80(4)	112(5)	99(2)
Eu2		0	0.54832(2)	1/4	104(4)	101(5)	125(5)	110(2)
Ni1	0.340(9)	0	0.7293(2)	1/4	123(28)	195(42)	138(40)	152(21)
Ni2		0	0.91173(5)	1/4	107(8)	73(9)	100(11)	93(4)
Sn1		0	0.97747(3)	1/4	210(5)	78(6)	69(6)	119(3)
Sn2		0	0.25017(4)	1/4	171(6)	298(9)	200(9)	223(4)
Sn3		0	0.38327(3)	1/4	65(5)	143(6)	139(8)	116(3)
Sn4		0	0.11667(3)	1/4	121(5)	158(7)	59(7)	113(3)
Sn5A	0.417(4)	0	0.6662(1)	1/4	–	–	–	117(3)
Sn5B	0.583(4)	0	0.68134(8)	1/4	–	–	–	117(3)

Table 2. Atomic coordinates and anisotropic displacement parameters for two crystals of $Eu_2Ni_{2-x}Sn_5$. All atoms lie on Wyckoff sites $4c$ 0 y 1/4 of space group *Cmcm*. U_{eq} is defined as one third of the trace of the orthogonalized U_{ij} tensor. $U_{12} = U_{13} = U_{23} = 0$.

Table 1. Crystal data and structure refinements for two crystals of $Eu_2Ni_{2-x}Sn_5$, *Cmcm*, $Z = 4$.

Empirical formula	$Eu_2Ni_{1.49(1)}Sn_5$	$Eu_2Ni_{1.35(1)}Sn_5$
Molar mass, g mol^{-1}	984.85	976.48
Unit cell dimensions, pm	$a = 466.03(4)$	$a = 466.11(9)$
(single crystal data)	$b = 3843.1(8)$	$b = 3820.1(8)$
	$c = 462.92(9)$	$c = 462.51(9)$
Volume, nm^3	$V = 0.8291$	$V = 0.8235$
ρ, g cm^{-3}	7.89	7.88
Crystal size, μm^3	$20 \times 40 \times 60$	$20 \times 60 \times 90$
Transm. ratio (max/min)	2.10	3.02
Radiation	– Mo K_α ($\lambda = 71.073$ pm) –	
μ, mm^{-1}	32.9	32.8
$F(000)$	1671	1655
θ range, deg	$2-30$	$2-30$
Range in *hkl*	$\pm 6, \pm 52, \pm 6$	$\pm 6, \pm 52, \pm 6$
Total no. reflections	3986	3446
Independent reflections / R$_{int}$	692 / 0.0249	695 / 0.0507
Reflections with $I \geq 2\sigma(I)$ / R$_\sigma$	523 / 0.0197	371 / 0.0716
Data / parameters	692 / 39	695 / 39
Goodness-of-fit on F^2	0.932	0.677
Final $R1$ / $wR2$ indices	0.0220 / 0.0439	0.0206 / 0.0338
[$I \geq 2\sigma(I)$]		
$R1$ / $wR2$ indices (all data)	0.0363 / 0.0469	0.0531 / 0.0358
Extinction coefficient	0.00046(4)	0.00092(3)
Largest diff. peak / hole, e Å^{-3}	1.86 / -1.53	1.01 / -1.22

sample was placed within a thin-walled PVC container at a thickness corresponding to about 10 mg Eu cm^{-2}.

Discussion

Crystal chemistry

The stannide $Eu_2Ni_{2-x}Sn_5$ crystallizes with a new structure type. It belongs to a larger family of struc-

Table 3. Interatomic distances [pm] in the $Eu_2Ni_{1.35(1)}Sn_5$ structure. Standard deviations are all equal or less than 0.7 pm. Extremely short distances that are affected by the split positions are listed in brackets.

Eu1:	4	Sn5B	328.3	Sn2:	2	Ni1	244.2
	4	Sn5A	334.0		2	Ni1	246.3
	1	Ni1	338.1		4	Sn2	328.3
	2	Sn4	340.8		2	Eu1	347.7
	2	Sn3	341.9		2	Eu1	348.0
	2	Sn2	347.7		2	Sn5B	349.2
	2	Sn2	347.9		2	Sn5B	351.3
	1	Ni2	358.8	Sn3:	2	Ni2	257.2
Eu2:	4	Sn1	342.8		2	Sn5A	298.5
	2	Sn3	349.0		4	Sn4	328.3
	2	Sn4	350.0		2	Sn5B	338.2
	2	Sn1	357.2		2	Eu1	341.9
	4	Ni2	362.1		2	Eu2	349.0
	2	Eu2	435.6	Sn4:	2	Ni2	255.5
Ni1:	1	Sn5B	[183.2]		2	Sn5A	300.1
	1	Sn5A	241.2		4	Sn3	328.3
	2	Sn2	244.2		2	Sn5B	339.6
	2	Sn2	246.3		2	Eu1	340.8
	1	Eu1	338.1		2	Eu2	350.0
	4	Ni1	364.4	Sn5A:	1	Sn5B	[58.0]
Ni2:	1	Sn1	251.2		1	Ni1	241.2
	2	Sn4	255.5		2	Sn3	298.5
	2	Sn3	257.2		2	Sn4	300.1
	1	Eu1	358.8		4	Eu1	334.0
	4	Eu2	362.1	Sn5B:	1	Sn5A	[58.0]
Sn1:	1	Ni2	251.2		1	Ni1	[183.2]
	2	Sn1	288.3		4	Eu1	328.3
	4	Eu2	342.8		2	Sn3	338.2
	2	Eu2	357.2		2	Sn4	339.6
					2	Sn2	349.2
					2	Sn2	351.3
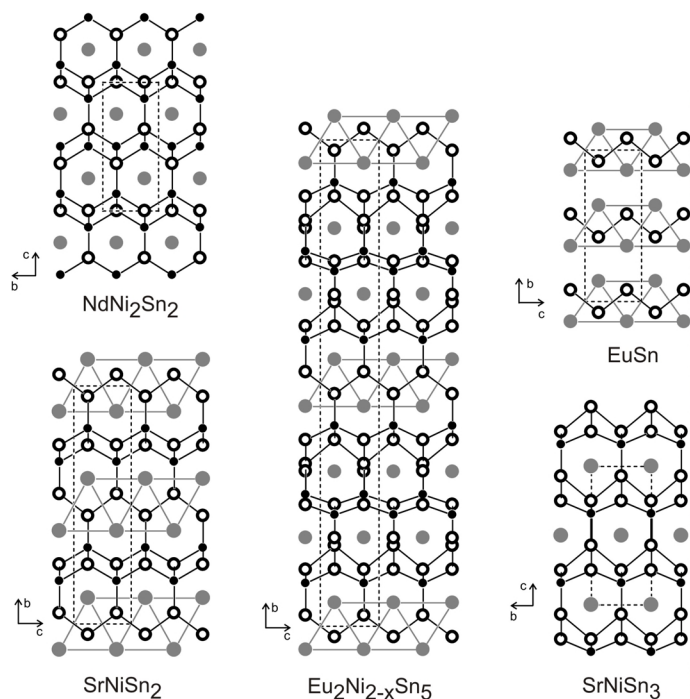
Fig. 1. Projection of the crystal structures of $NdNi_2Sn_2$ ($CaBe_2Ge_2$ type, *P4/nmm*) [23], $SrNiSn_2$ ($CeNiSi_2$ type, *Cmcm*) [24], $Eu_2Ni_{2-x}Sn_5$ (own type, this work), EuSn (CrB type, *Cmcm*) [25], and $SrNiSn_3$ ($BaNiSn_3$ type, *I4mm*) [17] along the short unit cell axis. Rare earth (alkaline earth), nickel and tin atoms are drawn as medium grey, black filled, and open circles, respectively. The three-dimensional $[Ni_xSn_y]$ networks are emphasized. For $SrNiSn_2$, $Eu_2Ni_{2-x}Sn_5$, and EuSn, the trigonal prismatic tin coordination is highlighted. For details see text.

tures with closely related structural slabs. In Fig. 1 we present projections of the $NdNi_2Sn_2$ ($CaBe_2Ge_2$ type, *P4/nmm*) [23], $SrNiSn_2$ ($CeNiSi_2$ type, *Cmcm*) [24], $Eu_2Ni_{2-x}Sn_5$ (own type, this work), EuSn (CrB type, *Cmcm*) [25], and $SrNiSn_3$ ($BaNiSn_3$ type, *I4mm*) [17] structures along the short unit cell axis. The ternary stannides all consist of three-dimensional nickel-tin networks with square-pyramidal $NiSn_5$ coordination in slightly different arrangements. These units are stacked with CrB-related units (tin zig-zag chains) in the structures of $SrNiSn_2$ and $Eu_2Ni_{2-x}Sn_5$. Such zig-zag chains occur in isolated form in the structure of EuSn (CrB type) [25].

The different connectivity patterns of the $NiSn_5$ square pyramids are presented in Fig. 2. In the $SrNiSn_3$ [17] structure, the $NiSn_5$ units are condensed *via* all four corners of the square ground plane, leading to layers where all apices point towards the $-c$ direction, a direct consequence for the non-centrosymmetricity of this structure. A double layer with up and down apices is realized in the centrosymmetric structure of $SrNiSn_2$ [24]. In both bases, the layers of condensed $NiSn_5$ pyramids are separated by strontium atoms. An even higher degree of connectivity is observed in the $NdNi_2Sn_2$ structure [23]. In the new structure type $Eu_2Ni_{2-x}Sn_5$, mono-layers and double-layers of

condensed $NiSn_5$ pyramids alternate, and these layers are charge-balanced and separated by the europium atoms.

The Ni–Sn distances within the complex $[Ni_{2-x}Sn_5]$ network of $Eu_2Ni_{2-x}Sn_5$ range from 241 to 257 pm. Most of these distances are shorter than the sum of the covalent radii [1] of 255 pm, indicating a substantial degree of Ni–Sn bonding. Besides the strong Ni–Sn bonds we also observe a variety of Sn–Sn interactions. The Sn–Sn distances cover the broad range from 288 to 351 pm. They compare well with the Sn–Sn distances in α-tin (281 pm) and β-tin (4×302 and 2×318 pm) [26]. The shortest Sn–Sn distance occurs within the Sn-Sn zig-zag chains. Cutouts of the chains in binary EuSn, and in $SrNiSn_2$ and $Eu_2Ni_{2-x}Sn_5$ are presented in Fig. 3. The Sn–Sn distances and the Sn–Sn–Sn angles show small differences, since they need to fit with the adjacent Ni-Sn slabs.

The two crystallographically independent europium sites Eu1 and Eu2 have 18 and 14 nearest Ni/Sn neighbors, respectively, in their coordination shells (Fig. 4). In the case of Eu2, two Eu2 atoms are capping the polyhedron, but with large Eu2–Eu2 distances of 436 pm, much longer than the Eu–Eu distance of 397 pm for the eight neighbors in elemental *bcc* europium [26]. Further europium neighbors are at the
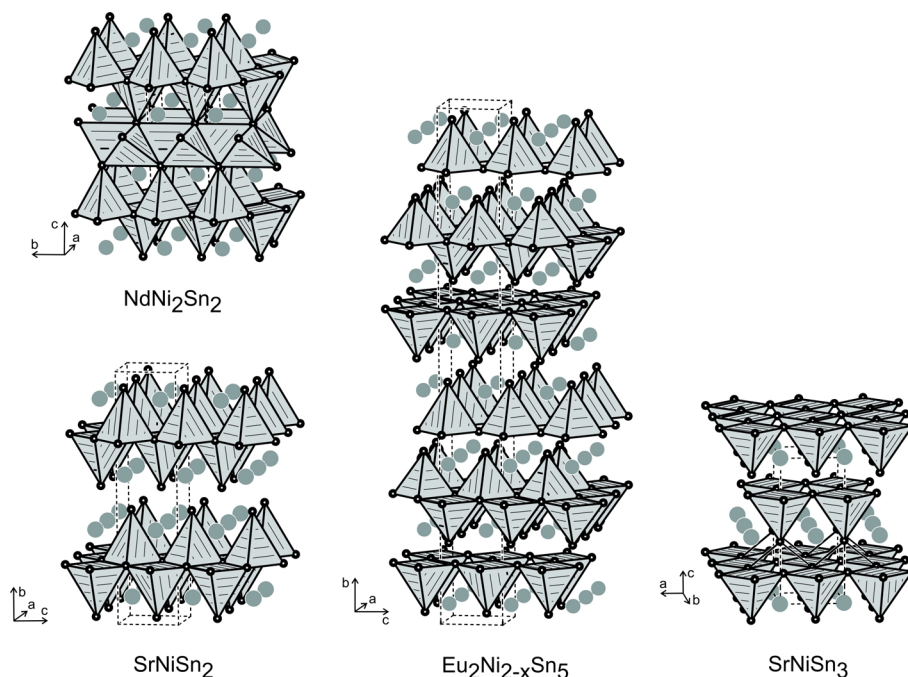
NdNi$_2$Sn$_2$

SrNiSn$_2$

Eu$_2$Ni$_{2-x}$Sn$_5$

SrNiSn$_3$

Fig. 2. The crystal structures of NdNi$_2$Sn$_2$ [23], SrNiSn$_2$ [24], Eu$_2$Ni$_{2-x}$Sn$_5$ (own type, this work), and SrNiSn$_3$ [17]. Rare earth (alkaline earth) and tin atoms are drawn as medium grey and open circles, respectively. The different networks of edge- and corner-sharing NiSn$_5$ square-pyramids are emphasized.
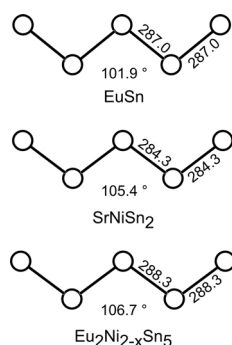

287.0   287.0
101.9 °
EuSn

284.3   284.3
105.4 °
SrNiSn$_2$

288.3   288.3
106.7 °
Eu$_2$Ni$_{2-x}$Sn$_5$

Fig. 3. Cutout of the tin zig-zag chains in the structures of SrNiSn$_2$ [24], Eu$_2$Ni$_{2-x}$Sn$_5$ (own type, this work), and EuSn [25]. Relevant interatomic distances and bond angles are indicated.

Eu1 4c ($m2m$)   Eu2 4c ($m2m$)

Fig. 4. Near-neighbor coordination of the europium atoms in the Eu$_2$Ni$_{2-x}$Sn$_5$ structure. Europium, nickel, and tin atoms are drawn as medium grey, black filled, and open circles, respectively.

anisotropic model   split model

Fig. 5. Coordination of the Ni1 atoms in the Eu$_2$Ni$_{2-x}$Sn$_5$ structure. For details see text.

longer distances of 463 and 466 pm, which correspond to the translation periods c and a.

Finally we draw back to the nickel deficits and the Sn5A/Sn5B split positions. In Fig. 5 we present the local Ni1 coordination with two models. The left-hand drawing emphasizes the extreme Sn5 dislocation for the anisotropic refinement, while the split refinement is shown on the right-hand side. For the Eu$_2$Ni$_{1.35(1)}$Sn$_5$ crystal the distance between the two split sites Sn5A and Sn5B is 58 pm. The split model can be rationalized in the following way. If the Ni1 site is filled, the Sn5A site is occupied, while the Sn5B position is occupied in the case of a Ni1 defect. Also the Sn2 atoms show enhanced U_{22} parameters (Table 2) since they are in close vicinity to the Ni1 atoms (Table 3).
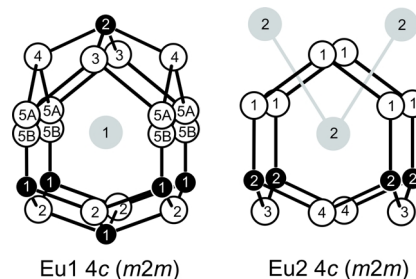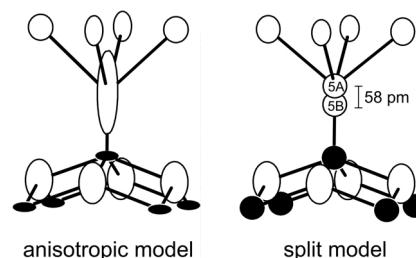
Since the Eu$_2$Ni$_{1.49(1)}$Sn$_5$ crystal showed an almost half occupied Ni1 site, at first sight, one might think of an ordered structure through superstructure forma-

Table 4. Fitting parameters for ^{151}Eu Mössbauer spectroscopic measurements on $Eu_2Ni_{1.50}Sn_5$: isomer shift (δ), electric quadrupole interaction (ΔE_Q), experimental line width (Γ), average magnetic hyperfine field ($\langle B_{eff} \rangle$), Gaussian standard deviation of B_{eff} (σ_B), and the intensity normalized to the Eu^{2+} area.

T (K)	δ (mm s^{-1})	Γ (mm s^{-1})	ΔE_Q (mm s^{-1})	$\langle B_{eff} \rangle$ (T)	σ_B (T)	Intensity (%)
78	−11.06(7)	2.67(3)	–	–	–	100
4.2	−10.64(7)	2.8[a]	−6.0(4)	21.2(2)	–	53(1)
	−10.7(1)	2.8[a]	−1.0(2)	11.5(4)	4.3(5)	47(1)

[a] Kept fixed during the fit.

tion. Nevertheless, careful examination of the reciprocal space gave no hint for superstructure reflections. Considering the data of the $Eu_2Ni_{1.35(1)}Sn_5$ crystal, it is clear that this structure has a homogeneity range, and especially for the lower nickel contents statistical occupancy occurs. This structural feature is well known for many of the $CeNiSi_2$-type phases [27 – 30]. Very low transition metal occupancies have been observed there as well, *e. g.* $LaFe_{0.34}Sn_2$ [27].

For the solid solution $Eu_2Ni_{2-x}Sn_5$ the occupancy of the Ni1 site has a direct consequence on the *b* lattice parameter. As is evident from Table 1, a decrease of the nickel content leads to a drastic decrease of the *b* parameter, while *a* and *c* are only marginally affected.

Mössbauer spectroscopy

Experimental and simulated ^{151}Eu Mössbauer spectra of the $Eu_2Ni_{1.50}Sn_5$ sample at 78 and 4.2 K are presented in Fig. 6. The corresponding fitting parameters are listed in Table 4. The two crystallographically independent europium atoms (Fig. 4) are both located on 4*c* Wyckoff sites. In addition, the defects present in the vicinity of the Eu1 site result in at least three spectroscopically independent Eu atoms in the structure. However, the spectrum in the paramagnetic range at 78 K is composed of only one resolved major resonance, which is a superposition as consequence of the chemical similarity of the different Eu species. From the isomer shift it can be concluded that both Eu atoms occur in a stable divalent state. But also a minor (~ 8 % intensity) component in the zero velocity vicinity is observed that can be attributed most likely to extrinsic Eu^{3+}, formed due to surface oxidation. Because of the superposition of the absorption lines, no information can be obtained regarding the quadrupolar interaction strengths that should be present because of the non-cubic site symmetries (*m2m*).

At 4.2 K the europium magnetic moments are close to that of an ordered state (*vide infra*) leading to magnetic hyperfine fields acting on the nuclear spin lev-
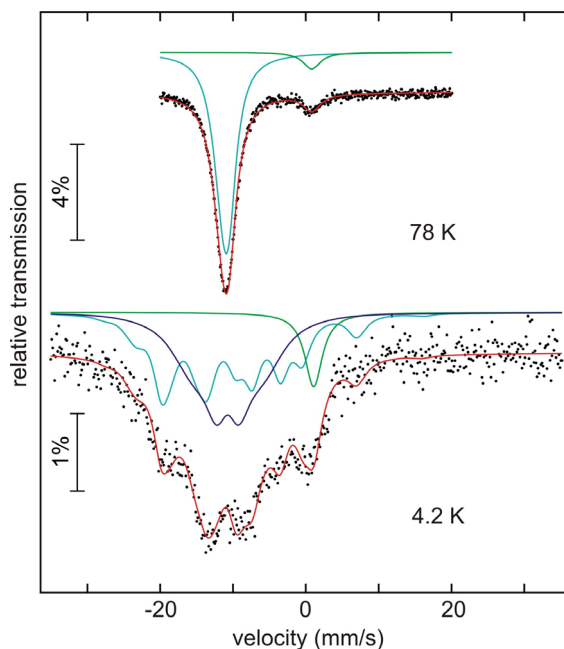

Fig. 6. Measured and simulated ^{151}Eu Mössbauer spectra of the $Eu_2Ni_{1.50}Sn_5$ sample at 78 and 4.2 K.

els resulting in clearly visible Zeeman splittings. In order to obtain a proper fit of the spectrum, two Eu^{2+} subspectra with an intensity ratio close to 1:1 with very similar isomer shift values have to be used. Furthermore a Gaussian distribution of magnetic hyperfine field strengths was introduced for the site, showing the significantly smaller $< B_{eff} >$ value. This resonance can therefore most likely be assigned to the Eu1 site, because the defects that are present in its coordination sphere could result in this B_{eff} distribution. Moreover, the extended Eu1–Eu1 distances of 463 pm when compared to Eu2–Eu2 (436 pm) could lead to the suppressed average magnetic hyperfine field strength, due to a weakened exchange interaction.

^{119}Sn Mössbauer spectra of $Eu_2Ni_{1.50}Sn_5$ at 78 and 4.2 K together with theoretical fits are presented in Fig. 7 and Table 5. The spectrum in the paramagnetic

Table 5. Fitting parameters for ^{119}Sn Mössbauer spectroscopic measurements on Eu$_2$Ni$_{1.50}$Sn$_5$: isomer shift (δ), average transferred magnetic hyperfine field ($\langle B_{Hf} \rangle$), electric quadrupole interaction (ΔE_Q), and experimental line width (Γ).

T (K)	δ (mm s^{-1})	Γ (mm s^{-1})	ΔE_Q (mm s^{-1})	$\langle B_{Hf} \rangle$ (T)
78	2.30(1)	1.28(1)	1.18(1)	–
4.2	2.31(1)	1.0^a	0.45(6)	3.17(2)

^{a} Kept fixed during the fit.
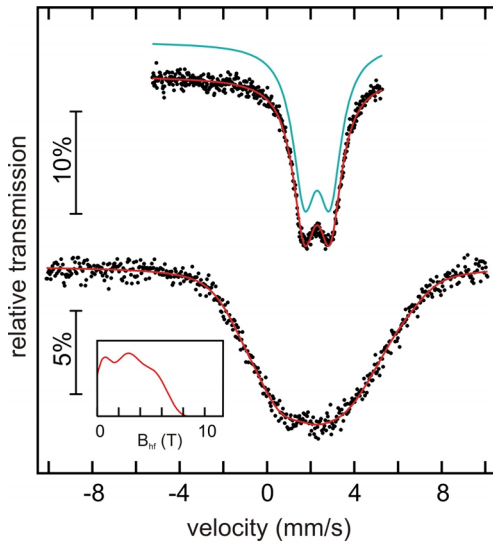

Fig. 7. Experimental and simulated ^{119}Sn Mössbauer spectra of the Eu$_2$Ni$_{1.50}$Sn$_5$ sample. The inset shows the magnetic hyperfine field distribution function.
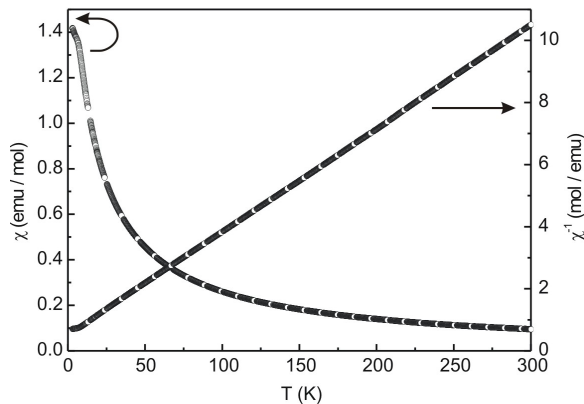

Fig. 8. Temperature dependence of the magnetic susceptibility (χ and χ^{-1} data) of the Eu$_2$Ni$_{1.50}$Sn$_5$ sample measured at 10 kOe.

range at 78 K consists of one superimposed signal, attributed to the five crystallographically independent tin atoms. Therefore the spectrum at 4.2 K showing
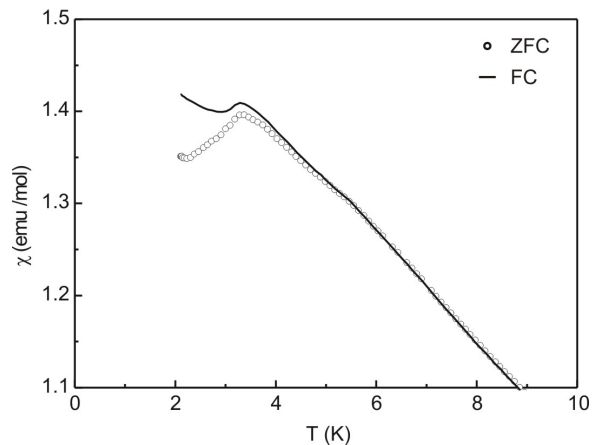

Fig. 9. Susceptibility measurement of the Eu$_2$Ni$_{1.50}$Sn$_5$ sample in a low external field of 100 Oe in the zero field cooling and field cooling mode.
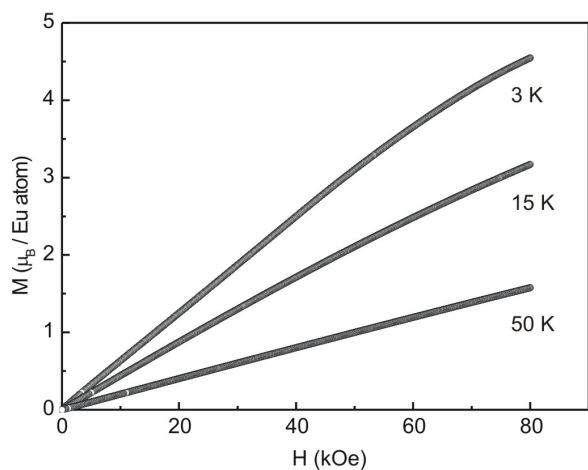

Fig. 10. Magnetization isotherms of the Eu$_2$Ni$_{1.50}$Sn$_5$ sample measured at 3, 15 and 50 K.

magnetical splitting was fitted utilizing a distribution of transferred magnetic hyperfine fields. The obtained distribution function reveals an average transferred hyperfine field of 3.17(2) T without any significant singularities.

Magnetic properties

The temperature dependence of the magnetic $\chi(T)$ and the inverse magnetic susceptibility $\chi^{-1}(T)$ of Eu$_2$Ni$_{1.50}$Sn$_5$ are displayed in Fig. 8, measured while warming in a *dc* field of 10 kOe after zero field cooling to 3 K. In the temperature range 50 – 300 K the compound shows Curie-Weiss behavior. A fit of the susceptibility data in this temperature range revealed an

effective magnetic moment of $\mu_{\text{eff}} = 7.74(1)\ \mu_{\text{B}}$ / Eu atom and a paramagnetic Curie temperature of $\theta_{\text{P}} = -14.1(5)$ K. The value of μ_{eff} is close to the theoretical free ion value of $7.94\ \mu_{\text{B}}$ for Eu^{2+}, indicating purely divalent europium. The θ_{P} value indicates that the magnetic interaction is of an antiferromagnetic type.

Fig. 9 shows the susceptibility measurement in a low external field of 100 Oe in the zero field cooling (ZFC) and field cooling (FC) mode. At around 3.5 K an anomaly, which can be attributed to antiferromagnetic ordering, is visible. This effect is suppressed at 10 kOe, and there is a visible bifurcation of $\chi(T)$ in the ZFC- and FC-mode. In conjunction with the aforementioned positional frustration of the Eu1 atoms, these findings hint towards a possible spin glass behavior of the compound. To corroborate this, further measure-ments, such as heat capacity, field-dependent *dc*- and frequency-dependent *ac*-susceptibility, studies are necessary.

The magnetization isotherms are shown in Fig. 10. At 50 K there is a linear increase of the magnetization with the applied external field as expected for a paramagnetic material. At 3 and 15 K the magnetization increases linearly at first and shows a slight curvature at higher field strengths. The highest magnetization reached at 3 K and 80 kOe was $4.54\ \mu_{\text{B}}$ / Eu atom, which is well below the theoretical value of $7\ \mu_{\text{B}}$ ($g_J \times S$).

[1] J. Emsley, *The Elements*, Oxford University Press, Oxford (U. K.) **1999**.

[2] H. A. Eick, N. C. Baenziger, L. Eyring, *J. Am. Chem. Soc.* **1956**, *78*, 5147.

[3] H. Bärnighausen, G. Brauer, *Acta Crystallogr.* **1962**, *15*, 1059.

[4] R.-D. Hoffmann, U. Ch. Rodewald, R. Pöttgen, *Z. Naturforsch.* **1999**, *54b*, 38.

[5] R. Pöttgen, D. Kußmann, *Z. Anorg. Allg. Chem.* **2001**, *627*, 55.

[6] B. Sendlinger, Dissertation, Universität München, München (Germany) **1993**.

[7] D. T. Adroja, S. K. Malik, *Phys. Rev. B* **1992**, *45*, 779.

[8] R. Pöttgen, *Z. Naturforsch.* **1996**, *51b*, 806.

[9] R. Müllmann, U. Ernet, B. D. Mosel, H. Eckert, R. K. Kremer, R.-D. Hoffmann, R. Pöttgen, *J. Mater. Chem.* **2001**, *11*, 1133.

[10] R.-D. Hoffmann, R. Pöttgen, D. Kußmann, D. Niepmann, H. Trill, B. D. Mosel, *Solid State Sci.* **2002**, *4*, 481.

[11] R. Pöttgen, R.-D. Hoffmann, R. Müllmann, B. D. Mosel, G. Kotzyba, *Chem. Eur. J.* **1997**, *3*, 1852.

[12] S. Esmailzadeh, R.-D. Hoffmann, R. Pöttgen, *Z. Naturforsch.* **2004**, *59b*, 1451.

[13] D. Kußmann, R. Pöttgen, U. Ch. Rodewald, C. Rosenhahn, B. D. Mosel, G. Kotzyba, B. Künnen, *Z. Naturforsch.* **1999**, *54b*, 1155.

[14] R. Pöttgen, D. Johrendt, *Chem. Mater.* **2000**, *12*, 875.

[15] D. Johrendt, G. Kotzyba, H. Trill, B. D. Mosel, H. Eckert, Th. Fickenscher, R. Pöttgen, *J. Solid State Chem.* **2002**, *164*, 201.

[16] R. Kraft, R.-D. Hoffmann, C. P. Sebastian, R. Pöttgen, Yu. Prots, W. Schnelle, M. Schmidt, Yu. Grin, *Chem. Mater.* **2008**, *20*, 1948.

[17] W. Dörrscheidt, H. Schäfer, *J. Less-Common Met.* **1978**, *58*, 209.

[18] R. Pöttgen, Th. Gulden, A. Simon, *GIT Labor-Fachzeitschrift* **1999**, *43*, 133.

[19] D. Kußmann, R.-D. Hoffmann, R. Pöttgen, *Z. Anorg. Allg. Chem.* **1998**, *624*, 1727.

[20] K. Yvon, W. Jeitschko, E. Parthé, *J. Appl. Crystallogr.* **1977**, *10*, 73.

[21] G. M. Sheldrick, SHELXS-97, Program for the Solution of Crystal Structures, University of Göttingen, Göttingen (Germany) **1997**.

[22] G. M. Sheldrick, SHELXL-97, Program for the Refinement of Crystal Structures, University of Göttingen, Göttingen (Germany) **1997**.

[23] V. A. Yartys, T. Olavesen, B. C. Hauback, H. Fjellvåg, *J. Alloys Compd.* **2002**, *336*, 181.

[24] V. Hlukhyy, S. Eck, T. F. Fässler, *Inorg. Chem.* **2006**, *45*, 7408.

[25] F. Merlo, M. L. Fornasini, *J. Less-Common Met.* **1967**, *13*, 603.

[26] J. Donohue, *The Structures of the Elements*, Wiley, New York (U. S. A.) **1974**.

[27] W. Dörrscheidt, G. Savelsberg, J. Stöhr, H. Schäfer, *J. Less-Common Met.* **1982**, *83*, 269.

[28] M. François, G. Venturini, B. Malaman, B. Roques, *J. Less-Common Met.* **1990**, *160*, 197.

[29] P. Schobinger-Papamantellos, J. Rodríguez-Carvajal, G. H. Nieuwenhuys, L. W. F. Lemmens, K. H. J. Buschow, *J. Alloys Compd.* **1997**, *262 – 263*, 335.

[30] A. Gil, B. Penc, E. Wawrzyńska, J. Hernandez-Velasko, A. Szytuła, A. Zygmunt, *J. Alloys Compd.* **2004**, *365*, 31.